Advanced Electronic Materials

ADVANCED ELECTRONIC MATERIALS Open Access

www.advelectronicmat.de

RESEARCH ARTICLE OPEN ACCESS

3D-Printed Supramolecular Eutectogels—Tunable Conductive Wires for Soft Electric Circuits

Tajmon T. Vadukoote[1] | Nathaniel Craft[1] | Alyssa-Jennifer Avestro[1,2] | David K. Smith[1]

[1]Department of Chemistry, University of York, York, North Yorkshire, UK | [2]Department of Chemistry, University of Oxford, Oxford, Oxfordshire, UK

Correspondence: David K. Smith (david.smith@york.ac.uk)

Received: 21 December 2025 | **Revised:** 27 January 2026 | **Accepted:** 10 March 2026

Keywords: 3D-printing | conductivity | deep eutectic solvents | gels | self-assembly | supramolecular

ABSTRACT

Supramolecular eutectogels based on 1,3:2,4-dibenzylidenesorbitol (DBS) derivatives as low-molecular-weight gelators (LMWGs) are 3D-printed via wet-spinning. Solubility and assembly kinetics play key roles in LMWG printability in a deep eutectic solvent (DES), a process facilitated by the addition of water. On drying, the printed gels lose some water content, reaching a stable composition for optimal, reproducible electronic properties. The printed supramolecular eutectogels have high conductivities of ca. 5.0 mS/cm, enabling them to be used as soft conductive wires in simple electronic circuits. Furthermore, depending on LMWG structure, they can be selectively reacted with Au(III) and loaded with gold nanoparticles, demonstrating the tunability of this supramolecular approach at the molecular scale. The ability to print functional conductive gels with curved and flexible structures indicates the potential of LMWG eutectogels in the fabrication of soft electronic circuitry with future applications in bionanoelectronics.

1 | Introduction

Conductive polymer gels that can be shaped and patterned, with tunable electrical and mechanical properties, open new avenues for next-generation soft nanoelectronic devices [1–3]. However, polymer gels can have inherent limitations such as processability, reproducibility and tunability, that can be overcome by the unique structural characteristics of supramolecular gels assembled from low-molecular-weight gelators (LMWGs) [4–11]. As such, there has been interest in developing LMWG-based gels as soft conductive materials [12–14]. These colloidal materials combine a solid-like self-assembled network and a liquid-like phase, with conductivity being achieved via three distinct mechanisms: (i) having a conductive solid-like network [15–19], (ii) loading the gel with conductive additives [20, 21], or (iii) using a conductive liquid-like phase [22]. This latter strategy is a powerful way of enhancing conductivity without compromising gel structure, enabling high ion mobilities, and has been used to develop gel electrolytes for energy technologies [23–27]. Ionic liquids have been used as a conductive liquid-like phase in supramolecular gels [28–30]. And recently, with an increased emphasis on sustainability, attention has begun to focus on ionic deep eutectic solvents (DESs) [31].

DESs were first developed by Abbott and co-workers, offering advantages like low vapor pressure, low flammability, biodegradability and sustainability [32–35]. They are typically formed by combining hydrogen bond donor (HBD) and acceptor (HBA) components to form a low-melting hydrogen-bonded complex. Many DESs have ionic components, enabling ionic conductivity. Gels formed in DESs are often referred to as 'eutectogels', and moving beyond established interest in polymeric eutectogels [36, 37], 'supramolecular eutectogels' based on LMWGs have also been reported. In early work, our group and that of D'Anna reported bulk 'heat-cool' self-assembled eutectogels based on 1,3:2,4-dibenzylidene sorbitol (DBS) and L-amino acids,

respectively [38, 39]. These gels had similar conductivities to the native DESs. Recently, the scope of supramolecular eutectogels has been significantly expanded [31, 40, 41]. Injectable supramolecular eutectogels compatible with cell culture have also been reported [42], indicating the potential biocompatibility of such materials.

In terms of creating sophisticated soft electronic systems, shaping gels has considerable importance, but this can remain challenging for LMWG gels [43–46], as a result of their dynamic nature and relative rheological weakness compared to polymeric systems. 3D printing is a potentially versatile way of generating and shaping gels in a precise and controlled manner [47–50]. Amongst the methods used to print gels, wet-spinning is increasingly powerful. This method extrudes a solution of LMWG dissolved in a good solvent into a bath of poor solvent (or coagulant) to trigger gel assembly [51–58]. Although supramolecular LMWG gels have previously been 3D-printed by wet-spinning, achieving conductive materials is rare. Stupp and co-workers used shear flow to manually extrude a dissolved peptide amphiphile into a coagulant calcium salt solution, fabricating gel noodles, which were then used to incorporate carbon nanotubes, which gave the material high conductivity when dried [59]. Tovar and co-workers went on to use this noodle technique to fabricate gel objects from thiophene-modified peptides and demonstrated that alignment of the nanofibres endowed the noodles with anisotropic conductivity properties, which were enhanced parallel to the direction of the fibres [60]. A similar approach was taken by Carrascosa, Martín and co-workers to co-assemble n-type and p-type nanofibres with alignment in order to enhance conductivity [61]. Recently, we used wet-spinning to 3D-print a hydrogel based on a 1,3:2,4-dibenzylidenesorbitol (DBS) derivative that was then loaded with gold nanoparticles (AuNPs), demonstrating modest conductivity (up to ca. 100 μS/cm), with the AuNP network formed within the gel playing an active role in supporting conductivity [62].

Although 3D-printing has been established for polymeric eutectogels [63–67], it has not been reported for LMWG eutectogels, probably owing to challenges concerning supramolecular gel stability and pattern reproducibility. Here, we use wet-spinning to create soft, flexible eutectogel 'wires' with considerably high conductivities (>1.0 mS/cm), approaching the higher levels of conductivity achieved by native (e.g., neural) tissue [68]. Progressing the state-of-the-art for LMWG eutectogels beyond bulk gel formation (i.e. by conventional heat-cool methods) to enable their spatially controlled printed assembly is a crucial step toward realizing conductive, sustainable supramolecular materials with applications in soft robotics, wearable bioelectronics, and healthcare technologies.

2 | Results and Discussion

2.1 | Bulk Eutectogels

The LMWGs studied here were DBS-CO_2Me, DBS-CO_2H, and DBS-$CONHNH_2$ (Figure 1A), synthesized by established procedures [69–71]. These DBS derivatives were initially used to prepare bulk eutectogels via a heat-cool methodology to determine the impact of the terminal groups on bulk eutectogel assembly. Based on our previous work with unfunctionalized DBS [38], we opted to employ the DES based on choline chloride (ChCl) and monoethylene glycol (MEG) (mixed in 1:2 molar ratio), also known as ethaline (Figure 1B). Although there has been some doubt as to the true DES status of ethaline [72], it remains widely used as a DES benchmark, is sustainable, and has suitable viscosity and conductivity for our desired application.

Pleasingly, all three LMWGs formed eutectogels, and we were delighted to find minimum gelation concentrations (MGCs) for DBS-CO_2Me, DBS-CO_2H, and DBS-$CONHNH_2$ of 0.4%, 0.6%, and 2.0% wt/vol, respectively. Notably, these MGCs are very significantly lower than unmodified DBS in ethaline (4.0% wt/vol), highlighting the benefit of tuning gelator structure for optimizing gel formulations [39]. Further, DBS-CO_2Me and DBS-CO_2H have lower MGCs than the previously reported best-in-class halogen-modified DBS derivatives (e.g., DBS-F, 1.6% wt/vol) [73]. Lower MGCs are desirable in terms of both cost and sustainability. We surmise that the lower solubility of the acid and ester derivatives in ethaline promotes assembly and lowers the MGC. DBS-$CONHNH_2$ is more soluble, likely due to its N—H groups acting as H-bond donors, facilitating interaction with components of the DES. Above certain loadings (i.e., their solubility limits), some LMWGs did not fully dissolve, even at elevated temperatures, and homogeneous gels could not be formed. For example, DBS-CO_2Me would not fully dissolve ≥3.0% wt/vol, and DBS-CO_2H ≥5.0% wt/vol. In contrast, although DBS-$CONHNH_2$ could not form gels at lower loadings on account of its greater solubility, it could be fully dissolved at higher loadings, even forming homogeneous gels at 5.0% wt/vol. These bulk gels were fully characterized for their rheological and electrical conductivity properties, confirming the utility of functionalized DBS-based LMWGs in eutectogels (see Supporting Information for full details).

2.2 | Optimization of Wet-Spinning for Eutectogels

Having established the ability of these DBS derivatives to form bulk eutectogels, we explored their wet-spinning in the DES. It is already known that DBS-CO_2H and DBS-$CONHNH_2$ can be wet-spun as hydrogels by injecting a DMSO solution into water [54, 55, 62]. LMWG solutions (1.0, 3.0, 5.0, 8.0 and 10% wt/vol) in DMSO were initially manually injected via a micropipette (250 μL) into 1 mL of ethaline (ChCl/MEG, 1:2 molar ratio) to assess gel filament formation (Figures S6 and S7), but no LMWGs formed continuous filaments. At higher concentrations (3.0%–10% wt/vol), DBS-CO_2Me samples formed bulk gels rather than filaments, reflecting uncontrolled assembly of this LMWG due to its lower solubility. As a further problem, the poor miscibility of DMSO solutions in the DES, and the absence of immediate gelation at the interface between solvents, led to LMWG solutions tending to float toward the surface of ethaline, preventing filament formation. Compared to using water as the coagulant, such logistical challenges observed with ethaline would have to be overcome to enable wet-spinning. Primarily, faster assembly and enhanced solvent miscibility were required, and we therefore decided to modify the coagulant to control these factors.

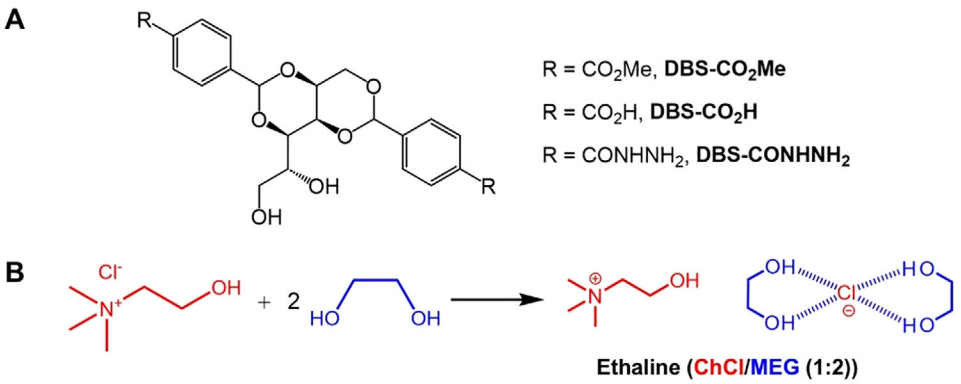

FIGURE 1 | (A) Structures of low-molecular-weight gelators (LMWGs) DBS-CO_2Me, DBS-CO_2H and DBS-$CONHNH_2$. (B) Structural representation of the ethaline system (ChCl: MEG, 1:2 molar ratio) used as a deep eutectic solvent (DES).

TABLE 1 | Optimization of solvent composition for wet-spinning of LMWGs from DMSO into water in ethaline mixtures.

		Water in Ethaline (% v/v)										
LMWG	Loading (% wt/vol)	0	10	20	30	40	50	60	70	80	90	100
DBS-$CONHNH_2$	1.5	X	X	X	X	X	X	X	✓	✓	✓	✓
	3.0	X	X	X	X	X	✓	✓	✓	✓	✓	✓
	4.5	X	X	X	X	✓	✓	✓	✓	✓	✓	✓
DBS-CO_2H	1.5	X	X	X	X	✓	✓	✓	✓	✓	✓	✓
	3.0	X	X	X	✓	✓	✓	✓	✓	✓	✓	✓
	4.5	X	X	✓	✓	✓	✓	✓	✓	✓	✓	✓

Using water as a co-solvent can trigger the assembly of a variety of bulk gels based on LMWGs [74–77]. We therefore decided to use ethaline/water mixtures to enhance the miscibility with the LMWG solutions in DMSO, as well as reducing LMWG solubility in the coagulant and hence promoting filament formation via a nucleation-like process. Water was expected to trigger rapid assembly, leading to both ethaline and water being retained within the resultant gel network (see below). We began by preparing DMSO solutions of the LMWGs at 1.5%, 3.0%, and 4.5% wt/vol and injected them into ethaline/water mixtures of varying ratios to optimize wet-spinning conditions (Figures S8–S17).

DBS-CO_2Me did not form gel filaments on wet-spinning at any LMWG loading or ethaline: water ratio, instead producing bulk gels and/or causing significant clogging of the injection nozzle. We attribute this to the very low water solubility of DBS-CO_2Me, meaning the presence of water induced uncontrolled assembly rather than controlled filament formation. Consequently, DBS-CO_2Me was not studied further. In contrast, effective filament formation was observed for DBS-CO_2H and DBS-$CONHNH_2$. Increasing LMWG concentration enhanced gel filament formation (Table 1). For example, when DBS-$CONHNH_2$ was wet-spun into 50% v/v water in ethaline, gel filaments were absent at 1.5% wt/vol, observed at 3.0% wt/vol and formed instantaneously at 4.5% wt/vol. Furthermore, raising the water content also favored filament formation, validating its use as a nucleating agent to trigger assembly (Table 1). The minimum water content in ethaline required for DBS-$CONHNH_2$ filament formation at a loading of 4.5% wt/vol was 40% v/v, whereas at 1.5% wt/vol, more water (70% v/v) was needed. Similar trends were observed for DBS-CO_2H, but filament formation was generally preferred. Indeed, DBS-CO_2H formed filaments at 1.5, 3.0, and 4.5% wt/vol, as long as at least 40% v/v water was present. Furthermore, at 4.5% wt/vol, filament formation was even triggered by 20% v/v water in ethaline. DBS-CO_2H, therefore required less water for filament formation than DBS-$CONHNH_2$, reflecting the lower solubility and MGC of the DBS-CO_2H eutectogel (see above).

After this preliminary manual study had identified DBS-$CONHNH_2$ and DBS-CO_2H as candidates for wet-spinning in ethaline/water, we optimized 3D-printing using an AxiDraw minikit 2 machine (Figure S1) under regulated conditions. In particular, we wanted to optimize filament integrity and the spatial resolution of the printed pattern, while maximising DES loading with a view to ionic conductivity.

An LMWG loading of 4.5% wt/vol in DMSO was selected, as in the preliminary work, this allowed for increased ethaline content in the coagulant bath (Table 1). The LMWG solution was passed through a 23G needle inserted into the ethaline/water mixture in a petri dish (6 cm diameter). Patterning was performed using a constant flow rate provided by a syringe pump (3.4 to 34 μL/min). The needle tip was kept at a height of 5 mm from the base of the petri dish. Two layers were printed, then the tip of the needle was raised by 0.17 mm; after printing every two layers, the needle

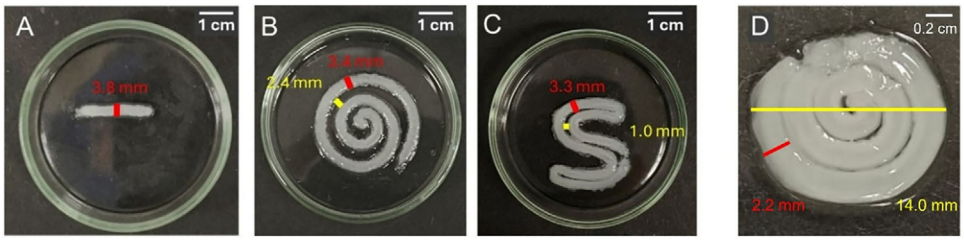

FIGURE 2 | (A) Single stripe (2 cm) printed using DBS-$CONHNH_2$ (4.5% wt/vol in DMSO) printed into ethaline: water (1:1) at a flow rate of 8.5 μL/min. (B) Spiral and (C) 'S' shaped design fabricated using DBS-$CONHNH_2$ (4.5% wt/vol in DMSO) printed into ethaline: water (1:1) at a flow rate of 8.5 μL/min, showcasing the ability to print curved geometries, with red and yellow lines indicating the thickness of the stripes and gaps, respectively. (D) Circular spiral using DBS-$CONHNH_2$ (4.5% wt/vol in DMSO) printed into ethaline: water (1:1) at a flow rate of 8.5 μL/min suitable for rheological testing. The spiral was created using the design in Figure S2. The red and yellow lines indicate the thickness and diameter of the printed spiral, respectively. The number of revolutions is ca. 3.

tip height was adjusted and printing was repeated. This process resulted in a spatially resolved gel pattern in which 16 filament layers were deposited on top of one another to create the 3D-printed object. We initially printed a simple, single stripe with a length of 2 cm (Figure 2A; Figures S18–S22).

Using 50% v/v water in ethaline, DBS-$CONHNH_2$ and DBS-CO_2H both formed well-defined filaments, but with different optimisation requirements (Table 2). DBS-$CONHNH_2$ could be effectively printed with flow rates of 8.5–11.9 μL/min. When printed at 8.5 μL/min, DBS-$CONHNH_2$ exhibited minimal spreading with an average stripe thickness of 3.7 mm. Increasing the flow rate to 10.2 and 11.9 μL/min led to slightly broader stripes (4.4 and 4.5 mm, respectively)—there is a little more spreading at faster flow rates as more material is delivered into the forming filament and spreads further from the injection site before gel assembly is complete. DBS-CO_2H followed a similar pattern but with slower optimal flow rates (6.8–10.2 μL/min). At 6.8 μL/min, DBS-CO_2H gave well-defined lines with an average width of 3.8 mm. Higher flow rates of 8.5 and 10.2 μL/min gave slightly increased spreading (4.0 and 4.3 mm, respectively). These observations reflect the previously discussed differences in the solvation of DBS-CO_2H and DBS-$CONHNH_2$, changing the assembly rate.

Using 90% v/v water in ethaline, faster self-assembly was induced by the large amount of water, allowing both LMWGs to be printed at significantly higher flow rates. For DBS-$CONHNH_2$, flow rates of 17.0 and 20.4 μL/min yielded objects with average thicknesses of 2.8 and 3.1 mm, respectively. DBS-CO_2H produced well-defined stripes at 11.9 and 13.6 μL/min, with thicknesses of 3.3 and 3.4 mm, respectively. Increasing the water content, therefore improves printing resolution by accelerating gelation, a process more marked for DBS-$CONHNH_2$. However, using 90% v/v water in ethaline also reduces the proportion of DES in the gel, which will compromise ionic conductivity. To maximize the amount of DES in the printed objects, we also tested wet-spinning DBS-CO_2H, which can tolerate more DES, using 30% v/v water in ethaline, but the much slower flow rate required for filament formation prevented effective printing.

In summary, at higher water content, rapid assembly enables faster flow rates without clogging, whereas for lower water content, slower flow rates were required to allow enough time for assembly. Printing gels at too fast a flow rate leads to detrimental pattern spreading as the printing rate outpaces gelation kinetics. Based on the results described above, our optimized conditions used an LMWG loading of 4.5% wt/vol in DMSO, injected at a flow rate of 8.5 μL/min into a coagulant bath comprising 50% v/v water in ethaline. This was applied for printing both DBS-$CONHNH_2$ and DBS-CO_2H, allowing direct comparison between LMWGs. These conditions provided a good balance between spatial resolution, filament integrity, and DES content.

To this point, we had focused on optimization by printing linear short stripes (Figure 2A). Next, we printed spiral and S-shaped designs (Figure 2B,C, respectively) to test the fabrication of flexible curved patterns and understand the spatial resolution at curve points (also see Figure S23). The designs were printed with good spatial resolution on the millimetre length-scale and excellent reproduction of curvature. In the spiral design, the width of the line is 3.4 mm, and the gap between lines is 2.4 mm. In the S-shaped design, the width of the line is 3.3 mm, and the gap between lines is 1.0 mm.

2.3 | Characterization of 3D-Printed Eutectogels

Performing rheology on 3D-printed gel stripes is challenging because they are not well suited to the geometry on a circular rheometer head, yet it is known that gel properties depend on fabrication method, so such characterization is important [78]. Therefore, to achieve the rheology of 3D-printed eutectogels, we devised a method in which gels were printed into a circular spiral with an overall final diameter of ca. 14 mm (Figure 2D; Figure S2) without significant gaps between spiral arms. These objects were trimmed prior to loading on the rheometer stage and were tested by standard oscillatory rheometry. In this way, rheometry was directly performed in a simple manner on the wet-spun gels without the need to use specialized techniques such as nanoindentation or cavitation rheometry, which provide a more localized view of network rheology. The rheology of these wet-spun spirals should not be directly compared with bulk gel discs, and we note here the potential difficulties caused by discontinuities in the structure. However, the data were reproducible across multiple runs, and we therefore believe it is a useful, simple way of comparing one wet-spun gel with another using a standard rheometer.

TABLE 2 | Optimization of flow rate for 3D-printing of LMWGs at a loading of 4.5% wt/vol in DMSO into ethaline: Water mixtures. Numerical values indicate the thickness of the stripe that was printed in each case (mm).

LMWG	Water in ethaline (% v/v)	Flow Rate (mL/min)										
		3.4	6.8	8.5	10.2	11.9	13.6	17.0	20.4	27.2	34.0	
$DBS\text{-}CONHNH_2$	50	X	X	3.7 mm	4.4 mm	4.5 mm	X	X	X	X	X	
	90	X	X	X	X	X	X	2.8 mm	3.1 mm	X	X	
$DBS\text{-}CO_2H$	50	X	3.8 mm	4.0 mm	4.3 mm	X	X	X	X	X	X	
	90	X	X	X	X	3.3 mm	3.4 mm	X	X	X	X	

For printed $DBS\text{-}CONHNH_2$ eutectogels, the G′ value was 1.5×10^5 Pa, with a G′/G″ crossover point of 1.6% (Figure S37). The printed $DBS\text{-}CO_2H$ eutectogels, on the other hand, exhibited somewhat lower stiffness, with $G' = 2.7 \times 10^4$ Pa, but higher strain tolerance (G′/G″ crossover of 8.0%) (Figure S38). Thus, by changing LMWG, the stiffness of the 3D-printed gel is decreased ca. 5-fold, while the elasticity (strain endurance) increases ca. 5-fold. This demonstrates how the molecular structure of LMWGs can significantly alter the mechanical characteristics of 3D-printed gels, emphasising the ease of tunability of this supramolecular approach. Importantly, unlike our previous printed hydrogels [58], no additional polymer was required to mechanically stabilize these printed eutectogels. As such, this is an LMWG-only approach to printed supramolecular materials.

To characterize the morphology of these wet-spun eutectogels at the nanoscale, we applied scanning electron microscopy (SEM). A drying step is required, and the presence of low volatility components in our DES, like ChCl, initially presented a problem, due to the tendency to crystallize/precipitate and dominate the SEM image. We therefore subjected printed eutectogels to solvent exchange, by placing the print in water, replacing it with fresh water every 2 h. After 6 h, solvent replacement was complete (as monitored via conductivity). We cannot rule out the possibility that the self-assembled LMWG scaffold may reorganize, although the presence of some water (ca. 50%) in the initial printed eutectogel, and the macroscopic stability of the gel throughout the solvent exchange, suggest that the integrity of the network structure is maintained. After solvent exchange, the printed objects were cryo-dried at liquid nitrogen temperature under high vacuum to limit drying-induced changes. Although artefacts can never be ruled out, all gels were prepared in the same way for imaging, enabling comparison between $DBS\text{-}CO_2H$ and $DBS\text{-}CONHNH_2$.

Nanofibrillar networks were clearly imaged, characteristic of controlled self-assembly (Figures 3; Figures S42 and S43), with fibre widths for $DBS\text{-}CONHNH_2$ of 55 ± 5 nm and for $DBS\text{-}CO_2H$ of 51 ± 5 nm. $DBS\text{-}CONHNH_2$ (Figure 3A) formed relatively straight, uniform fibres with smooth surfaces and limited bundling, whereas $DBS\text{-}CO_2H$ (Figure 3B) had a denser, more entangled morphology, with fibres appearing twisted and more irregular. This observation is consistent with our earlier observation that $DBS\text{-}CO_2H$ has lower water solubility and assembles more rapidly. The microstructure of $DBS\text{-}CO_2H$ observed by SEM had an evenly entangled network, whereas $DBS\text{-}CONHNH_2$ had microscale spherical clustered assemblies of nanofibers (Figure S44)—this morphological difference may explain the stiffer rheological properties of the $DBS\text{-}CONHNH_2$ 3D-printed gel.

As with our previously reported wet-spun hydrogel structures [54, 55, 62], we do not observe any evidence of nanofiber alignment, in contrast to the work of others, where pre-formed cylindrical micelles are extruded into a coagulant, leading to noodles with a degree of fiber alignment [57, 59–61]. This lack of alignment is expected, and reflects the fact that in our wet-spinning, the LMWG is dissolved as individual molecules in the DMSO solution, and there are no pre-existing nanostructures that can

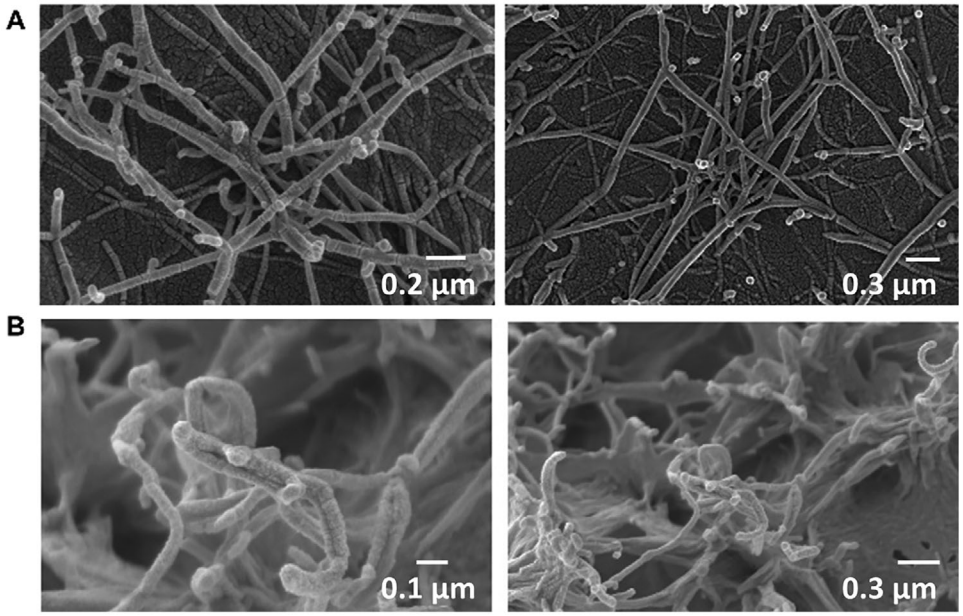

FIGURE 3 | SEM images of 3D-printed eutectogels after solvent-exchange and cryo-drying: (A) DBS-$CONHNH_2$ and (B) DBS-CO_2H.

be aligned by the shear forces experienced during extrusion. As such, the gel filaments formed in this case have structures that better reflect those of a bulk gel formed via a solvent switch methodology.

To further understand these 3D-printed objects, we explored their evolution upon drying. Given we were using 50% v/v water in ethaline as the wet-spinning medium, loss of any volatile components after printing could change the composition of the liquid-like phase in the printed eutectogel. In these printed eutectogels, water will be more volatile than either ChCl or MEG and thus would be expected to be lost more readily. We analyzed the 3D-printed eutectogel under various drying conditions. First, eutectogel stripes (4 cm) were dried under vacuum (150 mbar) for 2 h. The sample mass was checked every 10 min, and the weight loss was plotted (Figure S24). Printed samples of DBS-$CONHNH_2$ and DBS-CO_2H followed a similar trend, with a total weight loss of ca. 43%. Half of the weight loss occurred during the initial 10 min, and after ca. 50 min, weight loss was effectively complete. Alternatively, the gel stripes were left in ambient conditions for 6 h. As expected, drying was less significant, with a total weight loss of ca. 30% (Figure S25). Ambient drying was also slower than vacuum drying, with half the total weight loss taking ca. 50 min and requiring ca. 4 h to be effectively complete.

To analyze drying effects in more detail, the compositions of the 3D-printed eutectogels at different stages of vacuum drying were determined using ^{1}H NMR analysis (Figure 6; Figures S26 and S27). For 50% v/v water in ethaline, the theoretical amounts of H_2O, ChCl and MEG are 47.3, 27.9, and 24.6 wt.%, respectively. ^{1}H NMR studies performed on freshly printed DBS-$CONHNH_2$ (Figure 4A) and DBS-CO_2H (Figure 4B) eutectogel stripes before drying found compositional values in-line with theory, indicating the LMWGs do not preferentially interact with components of the printing medium or modify its composition. After 10 min vacuum drying, H_2O fell from 47.3 to 42.0 wt.% in DBS-$CONHNH_2$ and 34.6% in DBS-CO_2H. After complete drying, H_2O fell to ca. 17 wt.% in DBS-$CONHNH_2$ and 15 wt.% in DBS-CO_2H. The final solvent compositions of the DBS-$CONHNH_2$ and DBS-CO_2H gel stripes after vacuum drying were therefore ca. 15%–20% v/v water in ethaline. We also performed this NMR experiment on gel stripes dried under ambient conditions for 6 h and found water was reduced to 29.7 wt.% for DBS-$CONHNH_2$ and 26.2 wt.% for DBS-CO_2H, a similar composition to that obtained after 20 min of vacuum drying (Figures S27 and S28). This corresponds to ca. 25%–33% v/v water in ethaline. Slightly less water is lost from DBS-$CONHNH_2$ under both conditions, which might reflect the greater hydrogen bonding potential and water solubility of this LMWG, with such interactions holding onto H_2O slightly more effectively during the drying process. Importantly, in all cases, stable, reproducible compositions were achieved after sample drying.

In our previous work [62], when printed hydrogels were left to stand in ambient conditions even for a few hours, the water dried from the gels to such an extent that they became powders, losing their integrity. In contrast, in our present work, the non-volatility of the DES prevents complete drying, such that 3D-printed gels retain their mechanical stability and soft materials characteristics for days, affording significant potential in applications. Furthermore, the absence of any requirement for polymeric stabilizing additives means these 3D-printed eutectogels are wholly supramolecular systems.

2.4 | Conductivity of Eutectogels

We investigated eutectogel conductivity, hoping for conductivities in the mS/cm range as this would potentially unlock future applications in nanoelectronics or biomedicine [1–3]. The bulk eutectogels (see Supporting Information) exhibited excellent conductivities of ca. 11–12 mS/cm, slightly higher than the conductivity observed for pure ethaline (8.9 mS/cm).

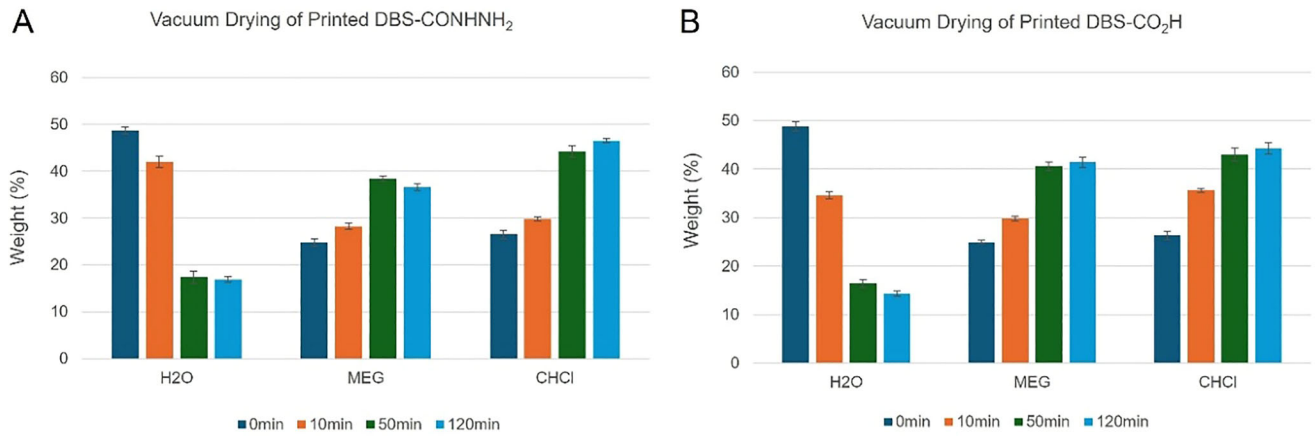

FIGURE 4 | Bar graphs indicating the composition of the liquid-like phase in 4 cm printed gel stripes in terms of wt.% of H_2O, monoethyleneglycol (MEG) and choline chloride (ChCl) on vacuum drying for different periods of time. (A) Gel stripe based on DBS-$CONHNH_2$; (B) Gel stripe based on DBS-CO_2H.

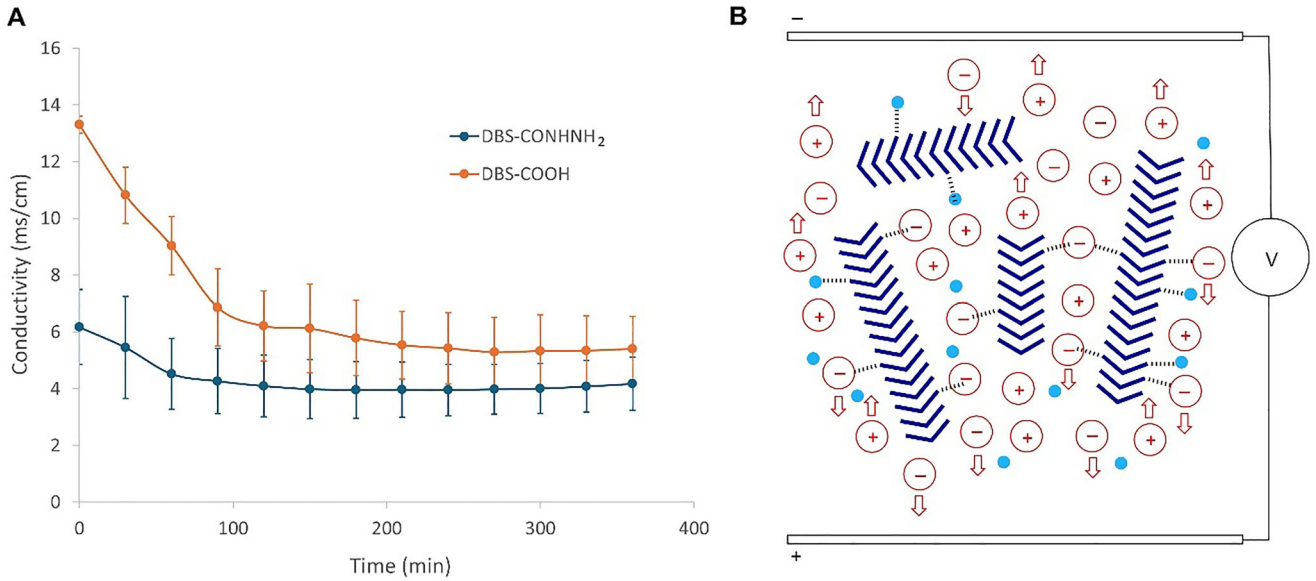

FIGURE 5 | (A) Time-dependent conductivity values of 3D-printed eutectogels prepared using DBS-$CONHNH_2$ and DBS-CO_2H in 1:1 ethaline/water mixtures, monitored over 6 h under ambient conditions using a four-probe setup. Conductivity values were recorded every 30 min. (B) Schematic of supramolecular eutectogels showing self-assembled LMWGs (dark blue V-shape), ionic components of DES (red and blue charged circles) and water (small pale blue circles). The movement of ions toward oppositely charged electrodes, responsible for the ionic conductivity mechanism, is indicated by red arrows. Proposed interactions between the self-assembled LMWGs and components of the conductive fluid, mediated by hydrogen bonds are indicated with black dashed lines.

There have been other reports of eutectogels with enhanced conductivity—it is argued that the gel network may facilitate ion transport via structural mechanisms [79–81].

To evaluate the electrical conductivity of 3D-printed eutectogels, 4 cm gel stripes were subjected to four-point-probe conductivity measurements under an alternating current to eliminate electrode resistance and polarization effects. The stripes were printed directly onto copper electrodes, which were subsequently connected to a conductivity meter (Figure S4). The DBS-CO_2H eutectogel displayed an initial conductivity of 13.3 (± 0.3) mS/cm, which stabilized after ca. 3.5 h in ambient conditions to a conductivity of 5.4 (± 1.1) mS/cm (Figure 5A). The DBS-$CONHNH_2$ eutectogel exhibited an initial conductivity of 6.7 (± 1.3) mS/cm, which stabilized after ca. 3 h, to 4.2 (± 0.9) mS/cm (Figure 5A). These values are in stark contrast to the previously reported DBS-CO_2H and DBS-$CONHNH_2$ hydrogels (wet-spun from DMSO at a loading of 1.5% wt/vol in the presence of 0.5% wt/vol agarose as a stabilizing agent), which displayed conductivities of just 28 and 14 μS/cm, respectively—a three order of magnitude difference [62].

The data suggest that in the freshly-printed eutectogel stripes, the presence of water enhances conductivity by lowering viscosity

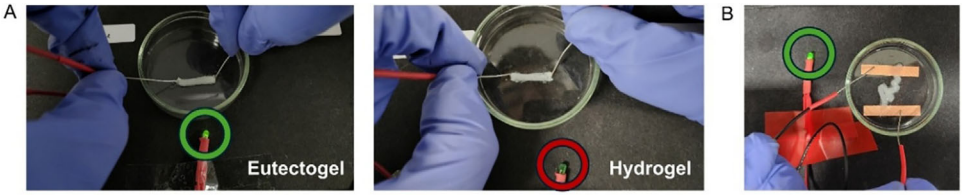

FIGURE 6 | (A) Visual demonstration of conductivity using a simple LED circuit: the DBS-$CONHNH_2$ eutectogel (left) completes the circuit and successfully lights the green LED, while the hydrogel (right) fails to do so, illustrating the enhanced conductivity imparted by the ethaline/water solvent system. (B) A curved 3D-printed DBS-$CONHNH_2$ eutectogel flexible pattern used to complete the same LED circuit, showing that the printed gel maintains conductivity even in a non-linear configuration, demonstrating its potential as a soft conductive element.

and assisting ionic mobility (see discussion below). This effect then reduces as the gel stripes dry. The enhanced conductivity of freshly-printed gels is more significant for DBS-CO_2H, which may reflect differences in the interactions of the self-assembled networks with the components of the liquid-like phase—indeed, DBS-$CONHNH_2$ is better able to hydrogen bond to DES/H_2O and hence limit initial conductivity. As the water evaporates from the printed stripes (see above), conductivity stabilizes at 5.4 mS/cm for DBS-CO_2H and ca. 4.2 mS/cm for DBS-$CONHNH_2$, leading us to conclude that the DES in the final dried printed eutectogel stripes is primarily responsible for the conductivity via an ionic mobility mechanism, with some influence of the LMWG structure in mediating this conductivity.

It is well-known that mixing water into DESs is an effective way of optimizing performance and modifies DES properties like viscosity and conductivity as a result of water solvating the ions in the DES [82–86]. Indeed, 'water-in-deep eutectic solvent gels' have been explored using polymer gelators because of their potential [87, 88]. The observed decrease in conductivity as the water component is reduced in our printed eutectogels is consistent with previous work investigating the conductivity of DES/water mixtures and supports the proposed mode of ionic conductivity (Figure 5B) [86]. Pleasingly, and importantly, the final equilibrated 3D-printed eutectogels are much more conductive (ca. 5 mS/cm) than our previous printed hydrogels based on the same LMWGs, which only had μS/cm conductivities [62].

2.5 | Using 3D-Printed Eutectogels in Simple Circuits

Having 3D-printed supramolecular eutectogels with high conductivities, we wanted to demonstrate their conductivity in a visual way. We therefore constructed a simple circuit using the printed gels as soft conducting elements. Single-stripe DBS-$CONHNH_2$ eutectogels (printed using 50% v/v water in ethaline as coagulant) and hydrogels (printed using H_2O as coagulant) were fabricated in separate petri dishes, and a normal wire with an attached 320 Ω resistor, 9 V battery and green LED were connected to opposite ends of both gel stripes (Figure 6A). When the circuit was completed using the 3D-printed eutectogel (mS/cm conductivity), the green LED illuminated. In contrast, connecting with the 3D-printed hydrogel (μS/cm conductivity) failed to activate the LED. This highlights the much improved conductivity achieved by replacing water with ethaline/water as a result of ionic conductivity.

To further explore the potential for shape-defined soft wiring, a more complex, curved eutectogel was printed and connected into the same circuit (Figure 6B). The green LED again illuminated, confirming the eutectogel maintained effective conductivity, demonstrating the potential of self-assembled LMWG eutectogels to serve as conductive components in rudimentary soft, flexible 3D-printed electronic circuitry.

2.6 | Loading 3D-Printed Eutectogels With Gold Nanoparticles (AuNPs)

To further demonstrate the versatility of 3D-printed LMWG eutectogels, we printed DBS-$CONHNH_2$ into 50% v/v water in ethaline in which $AuCl_3$ (0.4 mM) was dissolved (Figure 7A). Our previous work has demonstrated that, in water, a DBS-$CONHNH_2$ gel can reduce Au(III) to Au(0), creating gold nanoparticles (AuNPs) in situ within the gel (Figure 7B–E), increasing the conductivity ca. 8-fold from 14 to 114 μS/cm [54, 62, 89]. We were delighted to find that on printing into the solvent bath containing Au(III), printed gels loaded with AuNPs were directly fabricated. This is in contrast with our previous work printing into water, where the presence of Au(III) in the printing bath led to needle clogging, as AuNP formation was too rapid, with Au(III) having to instead be added once printing was complete [62]. Clearly, in ethaline/water mixtures, AuNP formation occurs at a slower rate than the printing of the gel stripes, allowing for the smooth direct printing of Au-loaded gels (Figure 7B–E illustrate the slow formation of AuNPs).

TEM was used to further characterize the AuNP-loaded gel stripe (Figure S45). It was found that the AuNPs had an average diameter of 33.6 ± 7.3 nm, somewhat larger than in our previously reported hydrogels [62], where the average diameter was ca. 20 nm. This difference likely reflects the slower formation of AuNPs in this DES system, meaning that fewer AuNPs are nucleated and then grow more slowly to larger sizes.

Interestingly, the AuNP-loaded DBS-$CONHNH_2$ eutectogel exposed to Au(III) had a higher initial conductivity of 16.0 (± 0.6) mS/ stabilizing to 7.0 (± 1.5) mS/cm after 3 h under ambient conditions, significantly higher than DBS-$CONHNH_2$ alone (Figure 7F). On the reduction of Au(III) into AuNPs, DBS-$CONHNH_2$ is itself oxidized to DBS-CO_2H [90]—it is interesting to note that the conductivity profile of the AuNP-loaded eutectogel is similar to that of the DBS-CO_2H eutectogel (Figure 5A). This would suggest that the change in LMWG induced by Au(III) reduction is primarily responsible for

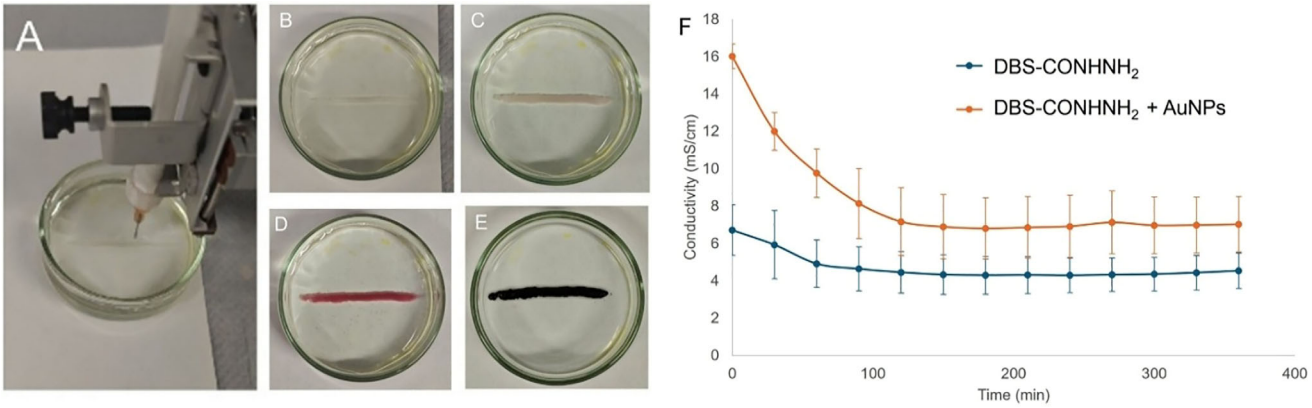

FIGURE 7 | (A) 3D printing of DBS-$CONHNH_2$ eutectogel into 0.4 mM $AuCl_3$ solution prepared in a 1:1 ethaline/water mixture. (B–E) Visual progress of in situ AuNP formation within the printed stripe over time: (B) 0 min, (C) 5 min, (D) 1 h, and (E) 24 h (F) Time-dependent conductivity of 3D-printed DBS-$CONHNH_2$ eutectogels with and without $AuCl_3$ (0.4 mM) over 6 h under ambient conditions.

the observed change in eutectogel conductivity. The conductivity values for the AuNP-loaded eutectogels were slightly higher than DBS-CO_2H alone, and it is possible that the presence of AuNPs slightly further enhances conductivity, although this change is within the error values. Given that in our previously reported hydrogels, AuNP-induced changes were only ca. 100 μS/cm, it is not surprising that any AuNP-induced increase is difficult to observe here. In such gels, the AuNPs are relatively distant from one another, and electron hopping would be required to establish a conductive pathway. TEM imaging (Figure S45) indicated that the AuNPs were not necessarily evenly or densely distributed throughout the eutectogel, which would make effective electron hopping difficult. It is therefore suggested that any enhancement in conductivity that could be induced by the presence of AuNPs is less efficient than the ionic conductivity mode that is possible for the native DES within these printed eutectogels.

In contrast, when a DBS-CO_2H gel stripe was printed into 50% v/v water in ethaline containing Au(III), we did not observe the colour change associated with AuNP formation (Figure S46A,B). This LMWG is not capable of reducing Au(III). The resulting materials had an initial conductivity of 17.0 (± 0.8) mS/cm, and after drying, the final stabilized conductivity was 5.6 (± 0.8) mS/cm (Figure S46C), similar to standard printed DBS-CO_2H.

Overall, this study demonstrates how chemical 'programming' of the LMWG can easily add functionality to these 3D-printed gels, in this case tuning the observed conductivity via changes in LMWG structure, and allowing the easy fabrication of a hybrid gel incorporating AuNPs. This ability to engineer function into materials via molecular-scale programming is a key advantage of the tunable LMWG approach to 3D-printed eutectogels. Intriguingly, we have previously reported that DBS-$CONHNH_2$ gels loaded with AuNPs are cytocompatible with human mesenchymal stem cells (hMSCs) and can actively promote the differentiation of hMSCs into bone cells [54, 91]. We therefore suggest the potential application of these 3D-printed AuNP-loaded conductive eutectogels as conductive biomaterials for future use in regenerative medicine.

3 | Conclusions

In this work, we have used DBS derivatives to 3D-print supramolecular eutectogels for the first time. None of the LMWGs could be printed directly into a DES, but the addition of water, to reduce solubility, enhance miscibility, and assist nucleation, allows DBS-CO_2H and DBS-$CONHNH_2$ to be wet-spun, each with different optimal conditions as a result of their solubilities and assembly kinetics. We fully characterized these wet-spun gels, which could be 3D-printed with mm-scale resolution, including in curved patterns. We also developed a 'spiral printing' method to match the shape of the gel to the standard parallel plate geometry in a rheometer and determine rheological performance. The printed gels lose water content on standing, or under vacuum, reaching a different composition in each case, which has gel-like characteristics and is stable for multiple days.

The 3D-printed gels are highly conductive, achieving stable conductivities of ca. 5.0 mS/cm, significantly higher than the μS/cm conductivities previously achieved by printed hydrogels (Figure 8) [21]. These conductivities enable the printed gels to be used as soft, conducting wires in a simple electronic circuit, lighting an LED once the circuit is completed by the gel. The ability to print stripes with curved structures highlights the potential of such materials in the fabrication of soft, flexible electronic circuitry.

The ability to tune the LMWG chemical structure, as well as controlling printability, makes it possible to incorporate additional functionality. We demonstrated that DBS-$CONHNH_2$ retains its unique ability to generate AuNPs in ethaline/water via in situ reduction, and that printing this LMWG directly into an Au(III) solution is a facile way of creating AuNP-loaded printed gels. Printed gels based on DBS-CO_2H do not facilitate this process.

In summary, shaping and patterning LMWG eutectogels by wet-spinning, in the absence of any polymeric stabilizing agent, enables the fabrication of robust, flexible, conductive, stable, soft, low-molecular-weight 3D-printed supramolecular systems. This may have applications in the emergent field of bionanoelectronics and wearable technologies—work in this direction is in progress.

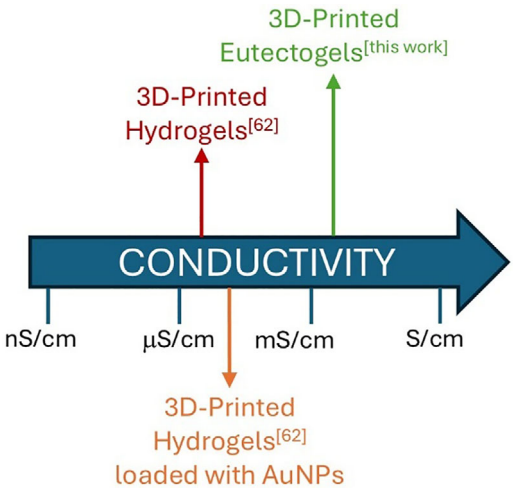

FIGURE 8 | Schematic diagram illustrating the conductivities achieved by printing LMWG hydrogels with and without AuNP-loading and eutectogels, illustrating the step change by printing eutectogels.

Acknowledgements

We thank the University of York Chemistry Wild Fund and Dr Tony Wild for supporting this research through the award of a PhD scholarship (T.T.V). Laboratory expenses were provided for N.C. by the University of York. A.-J.A. gratefully acknowledges The Royal Society for support with a Dorothy Hodgkin Research Fellowship (DHF\R1\180106) and Renewal Fellowship (DHF\R\231010). We also thank Dr Karen Hodgkinson, Paul Gunning, and Clare Steele-King (Department of Biology, University of York) for SEM imaging, and Chris Rhodes for assistance with reworking the conductivity setup and probe. We thank the reviewers for their input, which helped us significantly improve the manuscript.

Funding

This research was supported by the University of York Chemistry Wild Fund (PhD Scholarship, for TTV). Royal Society Dorothy Hodgkin Research Fellowship (DHF\R1\180106 and DHF\R\231010, for AJA).

Conflicts of Interest

The authors declare no conflicts of interest.

Data Availability Statement

All data are provided in the supporting information.

References

1. H. Yuk, B. Lu, X. Zhao, and H. Bioelectronics, "Hydrogel Bioelectronics," *Chemical Society Reviews* 48 (2019): 1642–1667, https://doi.org/10.1039/C8CS00595H.

2. H. Yuk, J. Wu, and S. Zhao, "Hydrogel Interfaces for Merging Humans and Machines," *Nature Reviews Materials* 7 (2022): 935–952.

3. H. Wang, W. Wang, and Z. Xie, "Patterning Meets Gels: Advances in Engineering Functional Gels at Micro/Nanoscales for Soft Devices," *Journal of Polymer Science* 60 (2022): 2679–2700, https://doi.org/10.1002/pol.20220148.

4. E. R. Draper and D. J. Adams, "Low-Molecular-Weight Gels: The State of the Art," *Chemistry* 3 (2017): 390–410, https://doi.org/10.1016/j.chempr.2017.07.012.

5. D. J. Adams, "Personal Perspective on Understanding Low Molecular Weight Gels," *Journal of the American Chemical Society* 144 (2022): 11047–11053, https://doi.org/10.1021/jacs.2c02096.

6. D. K. Smith, "Supramolecular Gels—A Panorama Of Low-Molecular-Weight Gelators From Ancient Origins to Next-Generation Technologies," *Soft Matter* 20 (2024): 10–70, https://doi.org/10.1039/D3SM01301D.

7. X. Yu, L. Chen, M. Zhang, and T. Yi, "Low-Molecular-Mass Gels Responding to Ultrasound and Mechanical Stress: Towards Self-Healing Materials," *Chemical Society Reviews* 43 (2014): 5346–5371, https://doi.org/10.1039/C4CS00066H.

8. C. D. Jones and J. W. Steed, "Gels With Sense: Supramolecular Materials That Respond to Heat, Light and Sound," *Chemical Society Reviews* 45 (2016): 6546–6596, https://doi.org/10.1039/C6CS00435K.

9. J. Li, L. Geng, G. Wang, H. Chu, and H. Wei, "Self-Healable Gels for Use in Wearable Devices," *Chemistry of Materials* 29 (2017): 8932–8952, https://doi.org/10.1021/acs.chemmater.7b02895.

10. S. Panja and D. J. Adams, "Stimuli Responsive Dynamic Transformations in Supramolecular Gels," *Chemical Society Reviews* 50 (2021): 5165–5200, https://doi.org/10.1039/D0CS01166E.

11. J. D. Simpson, L. Thomason, C. M. Woodley, et al., "Predicting the Mechanical Properties of Supramolecular Gels," *Advanced Materials* 37 (2025): 2415031, https://doi.org/10.1002/adma.202415031.

12. S. S. Babu, V. K. Praveen, and A. Ajayaghosh, "Functional π-Gelators and Their Applications," *Chemical Reviews* 114 (2014): 1973–2129, https://doi.org/10.1021/cr400195e.

13. O. Dumele, J. Chen, J. V. Passarelli, and S. I. Stupp, "Supramolecular Energy Materials," *Advanced Materials* 32 (2020): 1907247.

14. G. A. K. M. R. Bari, K.-H. Jeong, and H. R. Barai, "Conductive Gels for Energy Storage, Conversion, and Generation: Materials Design Strategies, Properties, and Applications," *Materials* 17 (2024): 2268.

15. B. W. Messmore, J. F. Hulvat, E. D. Sone, and S. I. Stupp, "Synthesis, Self-Assembly, and Characterization of Supramolecular Polymers From Electroactive Dendron Rodcoil Molecules," *Journal of the American Chemical Society* 126 (2004): 14452–14458, https://doi.org/10.1021/ja049325w.

16. J. Puigmartí-Luis, V. Laukhin, A. P. del Pino, et al., "Supramolecular Conducting Nanowires From Organogels," *Angewandte Chemie International Edition* 46 (2007): 238–241, https://doi.org/10.1002/anie.200602483.

17. S. Prasanthkumar, A. Saeki, S. Seki, and A. Ajayaghosh, "Solution Phase Epitaxial Self-Assembly and High Charge-Carrier Mobility Nanofibers of Semiconducting Molecular Gelators," *Journal of the American Chemical Society* 132 (2010): 8866–8867, https://doi.org/10.1021/ja103685j.

18. K. Sakakibara, P. Chithra, B. Das, et al., "Aligned 1-D Nanorods of a π-Gelator Exhibit Molecular Orientation and Excitation Energy Transport Different From Entangled Fiber Networks," *Journal of the American Chemical Society* 136 (2014): 8548–8551, https://doi.org/10.1021/ja504014k.

19. L. C. B. Salter, J. P. Wojciechowski, B. McLean, et al., "3,4-Ethylenedioxythiophene Hydrogels: Relating Structure and Charge Transport in Supramolecular Gels," *Chemistry of Materials* 36 (2024): 3092–3106.

20. S. Bhattacharya and S. K. Samanta, "Soft-Nanocomposites of Nanoparticles and Nanocarbons With Supramolecular and Polymer Gels and Their Applications," *Chemical Reviews* 116 (2016): 11967–12028, https://doi.org/10.1021/acs.chemrev.6b00221.

21. P. Choudhury, S. Dinda, and P. K. Das, "Fabrication of Soft-Nanocomposites From Functional Molecules With Diversified Applications," *Soft Matter* 16 (2020): 27–53, https://doi.org/10.1039/C9SM01304K.

22. K. Hanabusa, K. Hiratsuka, M. Kimura, and H. Shirai, "Easy Preparation and Useful Character of Organogel Electrolytes Based on Low Molecular Weight Gelator," *Chemistry of Materials* 11 (1999): 649–655, https://doi.org/10.1021/cm980528r.

23. N. Mohmeyer, P. Wang, H.-W. Schmidt, S. M. Zakeruddin, and M. Grätzel, "Quasi-Solid-State Dye Sensitized Solar Cells With 1,3:2,4-Di-O-Benzylidene-D-Sorbitol Derivatives as Low Molecular Weight Organic Gelators," *Journal of Materials Chemistry* 14 (2004): 1905–1909, https://doi.org/10.1039/B402324B.

24. Z. Huo, S. Dai, C. Zhang, et al., "Low Molecular Mass Organogelator Based Gel Electrolyte With Effective Charge Transport Property for Long-Term Stable Quasi-Solid-State Dye-Sensitized Solar Cells," *The Journal of Physical Chemistry B* 112 (2008): 12927–12933, https://doi.org/10.1021/jp8052168.

25. V. R. Basrur, J. Guo, C. Wang, and S. R. Raghavan, "Synergistic Gelation of Silica Nanoparticles and a Sorbitol-Based Molecular Gelator to Yield Highly-Conductive Free-Standing Gel Electrolytes," *ACS Applied Materials & Interfaces* 5 (2013): 262–267, https://doi.org/10.1021/am301920r.

26. L. Tao, Z. Huo, Y. Ding, et al., "Gel Electrolyte Materials Formed From a Series of Novel Low Molecular Mass Organogelators for Stable Quasi-Solid-State Dye-Sensitized Solar Cells," *Journal of Materials Chemistry A* 2 (2014): 15921–15930, https://doi.org/10.1039/C4TA02895C.

27. L. Tao, Z. Huo, Y. Ding, et al., "High-Efficiency and Stable Quasi-Solid-State Dye-Sensitized Solar Cell Based on Low Molecular Mass Organogelator Electrolyte," *Journal of Materials Chemistry A* 3 (2015): 2344–2352, https://doi.org/10.1039/C4TA06188H.

28. W. Kobo, S. Kambe, S. Nakade, et al., "Photocurrent-Determining Processes in Quasi-Solid-State Dye-Sensitized Solar Cells Using Ionic Gel Electrolytes," *The Journal of Physical Chemistry B* 107 (2003): 4374–4381, https://doi.org/10.1021/jp034248x.

29. N. Mohmeyer, D. Kuang, P. Wang, H.-W. Schmidt, S. M. Zakeeruddin, and M. Grätzel, "An Efficient Organogelator for Ionic Liquids to Prepare Stable Quasi-Solid-State Dye-Sensitized Solar Cells," *Journal of Materials Chemistry* 16 (2006): 2978–2983, https://doi.org/10.1039/B604021G.

30. J.-D. Decoppet, T. Moehi, S. S. Babkair, et al., "Molecular Gelation of Ionic Liquid–Sulfolane Mixtures, A Solid Electrolyte for High Performance Dye-Sensitized Solar Cells," *Journal of Materials Chemistry A* 2 (2014): 15972–15977, https://doi.org/10.1039/C4TA01995D.

31. G. A. L. e Souza, M. E. Di Pietro, and A. Mele, "Eutectic Solvents and Low Molecular Weight Gelators for Next-Generation Supramolecular Eutectogels: A Sustainable Chemistry Perspective," *RSC Sustainability* 2 (2024): 288–319, https://doi.org/10.1039/D3SU00264K.

32. A. P. Abbott, G. Capper, D. L. Davies, R. K. Rasheed, and V. Tambyrajah, "Novel Solvent Properties of choline Chloride/Urea Mixtures," *Chemical Communications* (2003): 70–71, https://doi.org/10.1039/b210714g.

33. A. P. Abbott, D. Boothby, G. Capper, D. L. Davies, and R. K. Rasheed, "Deep Eutectic Solvents Formed Between Choline Chloride and Carboxylic Acids: Versatile Alternatives to Ionic Liquids," *Journal of the American Chemical Society* 126 (2004): 9142–9147, https://doi.org/10.1021/ja048266j.

34. E. L. Smith, A. P. Abbott, and K. S. Ryder, "Deep Eutectic Solvents (DESs) and Their Applications," *Chemical Reviews* 114 (2014): 11060–11082, https://doi.org/10.1021/cr300162p.

35. B. B. Hansen, S. Spittle, B. Chen, et al., "J R Sangoro, Deep Eutectic Solvents: A Review of Fundamentals and Applications," *Chemical Reviews* 121 (2021): 1232–1285.

36. Y. Liang, Y. Tang, and W. Feng, "Non-Covalent Interactions in Action: Advancing Eutectogels for Enhanced Stability and Performance," *Polymer* 307 (2024): 127262.

37. A. Nicolau, A. L. Mutch, and S. C. Thickett, "Applications of Functional Polymeric Eutectogels," *Macromolecular Rapid Communications* 45 (2024): 2400405, https://doi.org/10.1002/marc.202400405.

38. S. Marullo, A. Meli, F. Giannici, and F. D'Anna, "Supramolecular Eutecto Gels: Fully Natural Soft Materials," *ACS Sustainable Chemistry & Engineering* 6 (2018): 12598–12602.

39. J. Ruiz-Olles, P. Slavik, N. K. Whitelaw, and D. K. Smith, "Self-Assembled Gels Formed in Deep Eutectic Solvents: Supramolecular Eutectogels With High Ionic Conductivity," *Angewandte Chemie International Edition* 58 (2019): 4173–4178, https://doi.org/10.1002/anie.201810600.

40. C. Esteves and A. C. A. Roque, "Short Peptide and Amino Acid-Based Supramolecular Ionogels and Eutectogels," *Chemistry—A European Journal* 30 (2024): 202400622, https://doi.org/10.1002/chem.202400622.

41. P. A. Mercadal, A. González, A. Beloqui, et al., "Eutectogels: The Multifaceted Soft Ionic Materials of Tomorrow," *JACS Au* 4 (2024): 3744–3758.

42. M. Criado-Gonzalez, N. Alegret, A. M. Fracaroli, et al., "Mixed Conductive, Injectable, and Fluorescent Supramolecular Eutectogel Composites," *Angewandte Chemie International Edition* 62 (2023): 202301489.

43. P. R. A. Chivers and D. K. Smith, "Shaping and Structuring Supramolecular Gels," *Nature Reviews Materials* 4 (2019): 463–478, https://doi.org/10.1038/s41578-019-0111-6.

44. H. S. Cooke, L. Schlichter, C. C. Piras, and D. K. Smith, "Double Diffusion for the Programmable Spatiotemporal Patterning of Multi-Domain Supramolecular Gels," *Chemical Science* 12 (2021): 12156–12164, https://doi.org/10.1039/D1SC03155D.

45. M. Dong, Y. Han, X. P. Hao, et al., "Digital Light Processing 3D Printing of Tough Supramolecular Hydrogels with Sophisticated Architectures as Impact-Absorption Elements," *Advanced Materials* 34 (2022): 2204333.

46. C. Tangsombun and D. K. Smith, "Fabricating Shaped and Patterned Supramolecular Multigelator Objects via Diffusion-Adhesion Gel Assembly," *Journal of the American Chemical Society* 145 (2023): 24061–24070, https://doi.org/10.1021/jacs.3c07376.

47. M. C. Nolan, A. M. Fuentes Caparros, B. Dietrich, et al., "Optimising Low Molecular Weight Hydrogels for Automated 3D Printing," *Soft Matter* 13 (2017): 8426–8432.

48. H. Jian, M. Wang, Q. Dong, et al., "Mechanical Properties and Degradability for 3D Bioprinting," *ACS Applied Materials & Interfaces* 11 (2019): 46419–46426.

49. A. M. Fuentes-Caparrós, Z. Canales-Galarza, M. Barrow, et al., "Mechanical Characterization of Multilayered Hydrogels: A Rheological Study for 3D-Printed Systems," *Biomacromolecules* 22 (2021): 1625–1638, https://doi.org/10.1021/acs.biomac.1c00078.

50. A. C. Farsheed, A. J. Thomas, B. H. Pogostin, and J. D. Hartgerink, "3D Printing of Self-Assembling Nanofibrous Multidomain Peptide Hydrogels," *Advanced Materials* 35 (2023): 2210378, https://doi.org/10.1002/adma.202210378.

51. A. Chalard, P. Joseph, S. Souleille, et al., "Wet Spinning and Radial Self-Assembly of a Carbohydrate Low Molecular Weight Gelator Into Well Organized Hydrogel Filaments," *Nanoscale* 11 (2019): 15043–15056, https://doi.org/10.1039/C9NR02727K.

52. A. Chalard, M. Mauduit, S. Souleille, P. Joseph, L. Malaquin, and J. Fitremann, "3D Printing of a Biocompatible Low Molecular Weight Supramolecular Hydrogel by Dimethylsulfoxide Water Solvent Exchange," *Additive Manufacturing* 33 (2020): 101162.

53. F. Andriamiseza, D. Bordignon, B. Payré, L. Vaysse, and J. Fitremann, "3D Printing of Biocompatible Low Molecular Weight Gels: Imbricated Structures With Sacrificial and Persistent *N*-Alkyl-D-Galactonamides," *Journal of Colloid and Interface Science* 617 (2022): 156–170, https://doi.org/10.1016/j.jcis.2022.02.076.

54. C. C. Piras, A. G. Kay, P. G. Genever, J. Fitremann, and D. K. Smith, "Self-Assembled Gel Tubes, Filaments and 3D-Printing With In Situ Metal Nanoparticle Formation and Enhanced Stem Cell Growth," *Chemical Science* 13 (2022): 1972–1981, https://doi.org/10.1039/D1SC06062G.

55. E. N. Drew, C. C. Piras, J. Fitremann, and D. K. Smith, "Wet-Spinning Multi-Component Low-Molecular-Weight Gelators to Print Synergistic Soft Materials," *Chemical Communications* 58 (2022): 11115–11118, https://doi.org/10.1039/D2CC04003D.

56. F. Andriamiseza, S. Peters, C. Roux, N. Dietrich, C. Coudret, and J. Fitremann, "Wet Spinning and 3D Printing of Supramolecular Hydrogels in Acid-Base and Dynamic Conditions," *Colloids and Surfaces A: Physicochemical and Engineering Aspects* 673 (2023): 131765, https://doi.org/10.1016/j.colsurfa.2023.131765.

57. D. McDowall, M. Walker, M. Vassalli, et al., "Controlling the Formation and Alignment of Low Molecular Weight Gel 'Noodles'," *Chemical Communications* 57 (2021): 8782–8785, https://doi.org/10.1039/D1CC03378F.

58. L. J. Marshall, M. Wallace, N. Mahmoudi, et al., "Hierarchical Composite Self-Sorted Supramolecular Gel Noodles," *Advanced Materials* 35 (2023): 202211277, https://doi.org/10.1002/adma.202211277.

59. S. Zhang, M. A. Greenfield, A. Mata, et al., "A Self-Assembly Pathway to Aligned Monodomain Gels," *Nature Materials* 9 (2010): 594–601, https://doi.org/10.1038/nmat2778.

60. B. D. Wall, S. R. Diedelmann, S. Zhang, et al., "Aligned Macroscopic Domains of Optoelectronic Nanostructures Prepared via Shear-Flow Assembly of Peptide Hydrogels," *Advanced Materials* 23 (2011): 5009–5014, https://doi.org/10.1002/adma.201102963.

61. J. López-Andarias, M. J. Rodriguez, C. Atienza, et al., "Highly Ordered *n/p*-Co-assembled Materials With Remarkable Charge Mobilities," *Journal of the American Chemical Society* 137 (2015): 893–897, https://doi.org/10.1021/ja510946c.

62. T. T. Vadukoote, A.-J. Avestro, and D. K. Smith, "3D-Printing Multi-Component Multi-Domain Supramolecular Gels With Differential Conductivity," *Angewandte Chemie International Edition* 63 (2024): 202409757.

63. C.-W. Lai and S.-S. Yu, "3D Printable Strain Sensors From Deep Eutectic Solvents and Cellulose Nanocrystals," *ACS Applied Materials & Interfaces* 12 (2020): 34235–34244, https://doi.org/10.1021/acsami.0c11152.

64. M. A. Smirnov, V. S. Fedotova, M. P. Sokolova, A. L. Nikolaeva, V. Y. Elokhovsky, and M. Karttunen, "Polymerizable Choline- and Imidazolium-Based Ionic Liquids Reinforced With Bacterial Cellulose for 3D-Printing," *Polymers* 13 (2021): 3044, https://doi.org/10.3390/polym13183044.

65. Y. Li, R. K. Kankala, L. Wu, A.-Z. Chen, and S.-B. Wang, "3D-Printed Photocurable Resin With Synergistic Hydrogen Bonding Based on Deep Eutectic Solvent," *ACS Applied Polymer Materials* 5 (2023): 991–1001, https://doi.org/10.1021/acsapm.2c01916.

66. G. Zhu, M. Liu, S. Weng, et al., "Dye-Free and Reprintable Multi-Color DLP 3D Printing Using $ZnCl_2$-Based Polymerizable Deep Eutectic Solvents and Type I Photoinitiators," *Chemical Engineering Journal* 472 (2023): 144987, https://doi.org/10.1016/j.cej.2023.144987.

67. A. L. Mutch, Y. Nahar, A. C. Bissember, et al., "Dissolve-on-Demand' 3D Printed Materials: Polymerizable Eutectics for Generating High Modulus, Thermoresponsive and Photoswitchable Eutectogels," *Macromolecular Rapid Communications* 45 (2024): 2400268.

68. C. Gabriel, A. Peyman, and E. H. Grant, "Electrical Conductivity of Tissue at Frequencies Below 1 MHz," *Physics in Medicine and Biology* 54 (2009): 4863–4878, https://doi.org/10.1088/0031-9155/54/16/002.

69. B. O. Okesola and D. K. Smith, "Versatile Supramolecular pH-Tolerant Hydrogels Which Demonstrate pH-Dependent Selective Adsorption of Dyes From Aqueous Solution," *Chemical Communications* 49 (2013): 11164–11166, https://doi.org/10.1039/c3cc45969a.

70. D. J. Cornwell, B. O. Okesola, and D. K. Smith, "Hybrid Polymer and Low Molecular Weight Gels—Dynamic Two-Component Soft Materials With Both Responsive and Robust Nanoscale Networks," *Soft Matter* 9 (2013): 8730–8736, https://doi.org/10.1039/c3sm51967h.

71. P. R. A. Chivers, J. A. Kelly, M. J. S. Hill, and D. K. Smith, "First-Generation Shaped Gel Reactors Based on Photo-Patterned Hybrid Hydrogels," *Reaction Chemistry & Engineering* 5 (2020): 1112–1117, https://doi.org/10.1039/D0RE00109K.

72. V. Agieienko and R. Buchner, "Is Ethaline a Deep Eutectic Solvent?," *Physical Chemistry Chemical Physics* 24 (2022): 5265–5268, https://doi.org/10.1039/D2CP00104G.

73. K. Fan, L. Wang, W. Wei, et al., "Multifunctional Self-Healing Eutectogels Induced by Supramolecular Assembly for Smart Conductive Materials, Interface Lubrication and Dye Adsorption," *Chemical Engineering Journal* 441 (2022): 136026, https://doi.org/10.1016/j.cej.2022.136026.

74. S. Lee, S. Oh, J. Lee, et al., "Stimulus-Responsive Azobenzene Supramolecules: Fibers, Gels, and Hollow Spheres," *Langmuir* 29 (2013): 5869–5877.

75. Y. Zhang, S. Li, M. Ma, et al., "Tuning of Gel Morphology With Supramolecular Chirality Amplification Using a Solvent Strategy Based on an Fmoc-Amino Acid Building Block," *New Journal of Chemistry* 40 (2016): 5568–5576, https://doi.org/10.1039/C6NJ00092D.

76. L. Liao, X. Jia, H. Lou, et al., "Supramolecular Gel Formation Regulated by Water Content in Organic Solvents: Self-Assembly Mechanism and Biomedical Applications," *RSC Advances* 11 (2021): 11519–11528.

77. N. K. McLeod, L. Stokes, J. Lewis, and D. K. Smith, "Supramolecular Gels With Potential Applications as Anti-Icing Agents," *Langmuir* 41 (2025): 13932–13947.

78. E. R. Draper and D. J. Adams, "Controlling Supramolecular Gels," *Nature Materials* 23 (2024): 13–15.

79. S. J. Bryant, M. A. da Silva, K. M. Z. Hossain, V. Calabrese, J. L. Scott, and K. L. Edler, "Non-Volatile Conductive Gels Made From Deep Eutectic Solvents and Oxidised Cellulose Nanofibrils," *Nanoscale Advances* 3 (2021): 2252–2260, https://doi.org/10.1039/D0NA00976H.

80. V. Gregorio, N. Garcia, and P. Tiemblo, "Ionic Conductivity Enhancement in UHMW PEO Gel Electrolytes Based on Room-Temperature Ionic Liquids and Deep Eutectic Solvents," *ACS Applied Polymer Materials* 4 (2022): 2860–2870, https://doi.org/10.1021/acsapm.2c00104.

81. B. Gu, W. Qin, G. Li, et al., "Tough, Strongly Adhesive, and Highly Conductive Eutectogels Enabled by Homogeneous and Stable Organic–Inorganic Hybrid Networks," *Chemical Engineering Journal* 522 (2025): 167541, https://doi.org/10.1016/j.cej.2025.167541.

82. C. Ma, A. Laaksonen, C. Liu, X. Lu, and X. Ji, "The Peculiar Effect of Water on Ionic Liquids and Deep Eutectic Solvents," *Chemical Society Reviews* 47 (2018): 8685–8720, https://doi.org/10.1039/C8CS00325D.

83. N. López-Salas, J. M. Vicent-Luna, S. Imberti, et al., "Looking at the "Water-in-Deep-Eutectic-Solvent" System: A Dilution Range for High Performance Eutectics," *ACS Sustainable Chemistry & Engineering* 7 (2019): 17565–17573, https://doi.org/10.1021/acssuschemeng.9b05096.

84. Y. Chen, D. Yu, W. Chen, L. Fu, and T. Mu, "Water Absorption by Deep Eutectic Solvents," *Physical Chemistry Chemical Physics* 21 (2019): 2601–2610, https://doi.org/10.1039/C8CP07383J.

85. I. Alfurayj, C. C. Fraenza, Y. Zhang, et al., "Solvation Dynamics of Wet Ethaline: Water Is the Magic Component," *The Journal of Physical Chemistry B* 125 (2021): 8888–8901, https://doi.org/10.1021/acs.jpcb.1c04629.

86. F. Lin, Z. Zuo, B. Cao, et al., "A Comprehensive Study of Density, Viscosity, and Electrical Conductivity of Choline Halide-Based Eutectic Solvents in H_2O," *Journal of Chemical & Engineering Data* 69 (2024): 4362–4376, https://doi.org/10.1021/acs.jced.4c00218.

87. Y. Chu, Q. Fan, C. Chai, et al., ""Water-in-Deep Eutectic Solvent" Gel Electrolytes Synergistically Controlled by Solvation Regulation and Gelation Strategies for Flexible Electronic Devices," *ACS Applied Materials & Interfaces* 15 (2023): 12088–12098, https://doi.org/10.1021/acsami.2c19928.

88. J. Deng, M. Chen, X. Zhang, et al., "Water-in-Eutectogel Electrolytes for Scalable Solid-State Electrochromic Devices," *Chemical Engineering Journal* 516 (2025): 163746.

89. B. O. Okesola, S. K. Suravaram, A. Parkin, and D. K. Smith, "Selective Extraction and In Situ Reduction of Precious Metal Salts From Model Waste To Generate Hybrid Gels With Embedded Electrocatalytic

Nanoparticles," *Angewandte Chemie International Edition* 55 (2016): 183–187, https://doi.org/10.1002/anie.201507684.

90. M. Albino, T. J. Burden, C. C. Piras, A. C. Whitwood, I. J. S. Fairlamb, and D. K. Smith, "Mechanically Robust Hybrid Gel Beads Loaded With "Naked" Palladium Nanoparticles as Efficient, Reusable, and Sustainable Catalysts for the Suzuki–Miyaura Reaction," *ACS Sustainable Chemistry & Engineering* 11 (2023): 1678–1689, https://doi.org/10.1021/acssuschemeng.2c05484.

91. C. Tangsombun, A. Simpson, P. G. Genever, and D. K. Smith, "Diffusion-Patterned Multi-Component Supramolecular Gels Loaded With Gold Nanoparticles Direct Mesenchymal Stem Cell Growth and Differentiation," *Advanced Healthcare Materials* 14 (2025): 2405057, https://doi.org/10.1002/adhm.202405057.

Supporting Information

Additional supporting information can be found online in the Supporting Information section.

Supporting File: aelm70346-sup-0001-SuppMat.docx.